

Original Research article

Characterization and Optimization of *Tamarindus indica* Copper Nanoparticles (Ta-Cunps) for the Adsorptive Removal of Malachite Green

Pampana Anil Kumar¹, Alpitha Suhasini J.², Sarva Rao B.³, Pulipati King¹, D. Appala Naidu¹ and Meena Vangalapati¹†

¹Department of Chemical Engineering, AUCE, Visakhapatnam, A.P, India

²Department of Chemical & Petroleum Engineering, UCEK, JNTUK, Kakinada, A.P, India

³Department of Chemical Engineering, MVGR, Vizianagaram, A.P, India

†Corresponding author: Meena Vangalapati; meenasekhar2002@yahoo.com

ORCID IDs of Authors: Pamapana Anil Kumar: <https://orcid.org/0009-008-6780-5889>;

J. A. Suhasini: <https://orcid.org/0000-0002-5399-2635>; Sarva Rao B: <https://orcid.org/0009-0000-3909-6511>;

Pulipati King: <https://orcid.org/0000-001-8210-3019>; D. Appala Naidu: <https://orcid.org/0000-0002-2355-4394>;

Meena Vangalapati: <https://orcid.org/0000-0002-7303-8160>

Key Words	Malachite Green, TA-CuNPs, Adsorption, Green synthesis, RSM-CCD
DOI	https://doi.org/10.46488/NEPT.2026.v25i03.B4401 (DOI will be active only after the final publication of the paper)
Citation for the Paper	Pampana, A.K., Alpitha, S.J., Sarva, R.B., Pulipati, K., Appala Naidu, D. and Vangalapati, M., 2026. Characterization and optimization of <i>Tamarindus indica</i> copper nanoparticles (Ta-Cunps) for the adsorptive removal of malachite green. <i>Nature Environment and Pollution Technology</i> , 25(3), B4401. https://doi.org/10.46488/NEPT.2026.v25i03.B4401

ABSTRACT

Copper nanoparticles doped with *Tamarindus indica seed* extract (TA-CuNPs) were green-synthesized to combine sustainability with enhanced the adsorption potential for wastewater treatment. Comprehensive characterization (SEM, FTIR, XRD, and BET) confirmed their porous structure and active surface functionalities. Batch adsorption of studies of Malachite Green (MG) demonstrated strong dependence on solution pH, adsorbent dosage, dye concentration, contact time, and temperature, with optimal performance at pH 6 and 0.5 g/L. The Langmuir isotherm provided the best equilibrium fit ($R^2 = 0.999$), yielding a monolayer capacity of 243.90 mg/g. Kinetic evaluation confirmed that pseudo-second-order dominance ($R^2 = 0.999$), indicating chemisorption, while thermodynamic analysis revealed that spontaneous and endothermic uptake ($\Delta G^\circ < 0$; $\Delta H^\circ > 0$). RSM-CCD optimization identified the ideal operational conditions: 19.85 mg/L MG, 0.498 g/L adsorbent, pH 6.18, and 318 K achieving maximum removal efficiency with excellent model accuracy ($R^2 > 0.98$; low error statistics). These results collectively establish TA-CuNPs as a high-capacity, green-synthesized, and scalable adsorbent suitable for practical wastewater treatment.

INTRODUCTION

Synthetic dyes are now major aquatic pollutants due to the textile industry's rapid expansion, which has increased wastewater discharge contaminated by dyes [Ahmad & Kumar, 2010]. Strong structural stability and resistance to degradation are characteristics of Malachite Green (MG), a highly persistent cationic dye used extensively in textiles, aquaculture, food processing, and disinfectants. Because of its environmental persistence, it can bioaccumulate and cause carcinogenic, mutagenic, and reproductive toxicity in humans and aquatic organisms [Chowdhury et al., 2011; Agarwal et al., 2012; Hussien Hamad & M.T.M, 2023].

While many remediation methods have been investigated, including photo-catalysis, oxidation, membrane filtration, and biological treatments, many of them have high operating costs, produce sludge, or are ineffective against stable dyes. Because of its simplicity, low cost, and high efficiency, adsorption continues to be the most reliable and cost-effective method for eliminating persistent organic contaminants [Jain et al., 2007; Ahmad & Kumar, 2010].

A variety of nanomaterials have demonstrated strong adsorption potential, including ZnS–Cu/AC composites [Dastkhon et al., 2015], iron-loaded ash [Agarwal et al., 2016], and pomegranate-peel-supported zero-valent iron nanoparticles [Gunduz & Bayrak, 2018], cellulose–Ag nanofibers [Nagalakshmi et al., 2021], and modified bentonite [Bishwas et al., 2023] etc., their high surface area, reactivity, and tunable surface chemistry make nanomaterials appealing adsorbents; however, challenges remain regarding synthesis cost, environmental safety, and scalability.

Green synthesis has emerged as a sustainable alternative to conventional chemical routes, utilizing plant extracts as natural reducing and stabilizing agents to eliminate toxic reagents [Nadagouda, 2010; Shahwan et al., 2011]. Recent plant-mediated syntheses including *Hibiscus rosa-sinensis* (Au, Ag) [Philip, 2010], *sorghum bran* (Fe, Ag) [Njagi, 2011], *Terminalia chebula* (Pd, Fe) [Kumar, 2013], and *Grevillea robusta* (Ag) [Poiba et al., 2023] etc., demonstrate the feasibility, biocompatibility, and environmental safety of these approaches. Coupled with low-cost techniques such as co-precipitation, green nanomaterials offer promising pathways for sustainable wastewater treatment [Bashanaini, 2019; Sowjanya et al., 2023].

No previous study has reported the synthesis of TA–CuNPs using *Tamarindus indica* seed extract for MG removal, nor evaluated their adsorption behavior using integrated kinetic, thermodynamic, and RSM-CCD optimization. The present study investigates the influence of pH, initial dye concentration, adsorbent dosage, contact time, and temperature on MG removal; evaluates adsorption kinetics, isotherms, and thermodynamics; and applies RSM-CCD to optimize process conditions. This work contributes to sustainable wastewater treatment by demonstrating a low-cost, bio-derived nanomaterial with high adsorption efficiency and strong potential for scale-up.

2. MATERIALS AND METHODS

2.1. Production of *Tamarindus indica* seed-Doped Copper Nanoparticles (TA-CuNPs)

To ensure a high availability of phytochemicals that may serve as reductants and capping agents, a concentrated *Tamarindus indica* seed extract was prepared. Since concentrated plant extracts were proven for rapid metal-ion reduction during the synthesis of green nanoparticles, the high solid–liquid ratio was intentionally employed. Specifically, 50 g of ground seed powder was suspended in 250 mL of distilled water and heated to 80°C for 60 minutes using a hot-plate heater equipped with magnetic stirring. To get a clarified extract, the mixture was filtered. In order to create nanoparticles, 5 mL of the extract was added dropwise to 50 mL of a newly made 0.005 M $\text{CuSO}_4 \cdot 2\text{H}_2\text{O}$ solution while being continuously stirred at an ambient temperature. The reaction was allowed to proceed for 30 min, during which the transition from a light to a dark brown coloration provided qualitative confirmation of Cu^{2+} reduction and nanoparticle formation. The suspension was subsequently centrifuged at 4250 rpm for 30 min to recover the solid phase. After being dried for 12 hours at 373 K in a hot-air oven, the separated

material was carefully ground into a uniform powder. Since the study used a low-temperature green synthesis method to preserve phytochemical functional groups, no calcination was carried out. Before characterization and adsorption tests, the finished product was kept in airtight containers under carefully regulated laboratory conditions ($25 \pm 2^\circ\text{C}$, low ambient humidity).

2.2. Batch Adsorption Experiments

Under experimental conditions, the batch adsorption performance of TA-doped copper nanoparticles (TA-CuNPs) toward malachite green (MG) was methodically examined. Each trial involved adding 0.4 g of TA-CuNPs to 100 mL of MG solution (20–100 mg/L) in 250 mL Erlenmeyer flasks, which were then shaken at 150 rpm for 5–60 minutes using a temperature regulated orbital shaker kept at 308 K. Using 0.1 M HCl or NaOH, the pH of the solution was adjusted between 3 and 8, and pH stability was confirmed both before and after each experiment. Every adsorption test was performed in triplicate, and to account for any non-adsorptive losses, the proper blanks (MG solution without adsorbent) were employed.

Following adsorption, the suspensions were centrifuged at 4000 rpm for 15 min, and the supernatant was filtered through 0.45 μm membrane filters prior to analysis. The residual MG concentration was quantified using a UV–Vis spectrophotometer at $\lambda_{\text{max}} = 423 \text{ nm}$ with a 1 cm quartz cuvette. Adsorption capacity/ dye uptake (q_e) and removal efficiency (%) were calculated using Eqs. (1) and (2) [R K Bishwas et al., 2023; Sowjanya B et al., 2023]:

$$\% \text{ Adsorption/Removal of dye} = \left(\frac{C_o - C_t}{C_o} \right) \times 100 \quad (1)$$

$$\text{Adsorption capacity/Dye uptake } q_e = \left(\frac{C_o - C_t}{m^*} \right) \times V \quad (2)$$

Where V (in L) is the solution's volume, m^* (in g) is the adsorbent's mass, and C_o and C_t (in mg/L) shows the initial and equilibrium MG dye concentrations. The adsorption mechanism was then clarified by using these experimental results for kinetic, isotherm, and thermodynamic modeling.

2.3. Kinetic, Equilibrium, and Thermodynamic Analyses of MG Adsorption

Employing the pseudo-first-order and pseudo-second-order models, the adsorption kinetics of Malachite Green (MG) onto TA–Cu–NPs were assessed to elucidate the rate-governing mechanism. In the pseudo-first-order model, adsorption is described by the difference between uptake at time t (q_t) and equilibrium uptake (q_e), where q_e values were experimentally determined from independent equilibrium adsorption trials conducted under identical conditions (Dastkhooon et al., 2015). The pseudo-second-order model attributes the rate to chemisorption, involving electron sharing or transfer between MG molecules and functional groups present on the nanoparticle surface (Mortazavi et al., 2016). All kinetic parameters were obtained using non-linear regression, as this approach minimizes systematic errors associated with linear transformations and provides more robust fits to experimental data. To find the best kinetic representation, both models were evaluated using the statistical indices R^2 , RMSE, and χ^2 .

The equation of Pseudo-first-order kinetics: $\ln(q_e - q_t) = \ln q_e - k_1 t$ (3)

The equation of Pseudo-second-order kinetics: $\frac{t}{q_t} = \frac{1}{k_2 q_e^2} + \frac{t}{q_m}$ (4)

Here, t is in time, it represents the adsorption time, while the pseudo-first-order and pseudo-second-order kinetic models, the rate constants are indicated by the k_1 and k_2 , respectively.

Using the Langmuir and Freundlich isotherm models, the equilibrium uptake of MG onto TA–Cu–NPs was evaluated at 318 K to determine the monolayer adsorption capacity and to characterize the surface heterogeneity of the nanoparticles. The

Freundlich model is more applicable in non-ideal situations because it allows adsorption on heterogeneous surfaces with variable energies, in contrast, the Langmuir model presupposes monolayer adsorption on a homogeneous surface with a limited quantity of identical sites. [Jain, R., et al., 2007].

$$\text{The expression for the Langmuir model: } q_e = \frac{q_{\max} K_L C_e}{1 + K_L C_e} \quad (5)$$

Where: q_e (in mg/g) is the adsorption capacity at equilibrium condition, C_e (in mg/L) is the dye concentration at equilibrium, q_{\max} (in mg/g) it stands for the highest monolayer adsorption capacity, and K_L (in L/mg) denotes adsorption constant of Langmuir, and it reflects the affinity of the adsorbent & adsorbate.

$$\text{The equation for the Freundlich model is written as: } q_e = K_f C_e^{1/n} \quad (6)$$

Where: “ K_f ” (mg/g).(mg/L)⁻ⁿ represents the constant of Freundlich, it indicates the adsorption capacity, and “n” stands for the heterogeneity factor, which provides insight into the intensity of adsorption and adsorbent surface irregularity.

The key parameters of thermodynamics, namely change in Gibbs free energy (ΔG°), enthalpy change in enthalpy (ΔH°), and change in entropy (ΔS°), were measured over the temperature range 303–318 K to clarify the characteristics and feasibility of the adsorption process. Comprehending the system's spontaneity and energetic characteristics, the dimensionless equilibrium constant ($K_c = q_e/C_e$) was calculated by dividing the dye's equilibrium concentration in the solution by the amount adsorbed on the nanoparticles, providing the basis for evaluating ΔG° and related thermodynamic behavior. Using the following relationship, the standard free energy change was calculated:

$$\Delta G^\circ = -RT \ln(K_c) \quad (7)$$

Where: T (in K) is the absolute temperature and R (in 8.314 J/mol. K) is the universal gas constant. The following linearized form of expression was used to estimate the values of ΔS° and ΔH° from the intercept and slope of the Van't Hoff plot.

$$\ln K_c = \frac{\Delta S^\circ}{R} - \frac{\Delta H^\circ}{RT} \quad (8)$$

This analysis shed light on the disorder, heat changes, and spontaneity related to MG adsorption onto TA-Cu-NPs.

2.4. Response Surface Methodology (RSM)

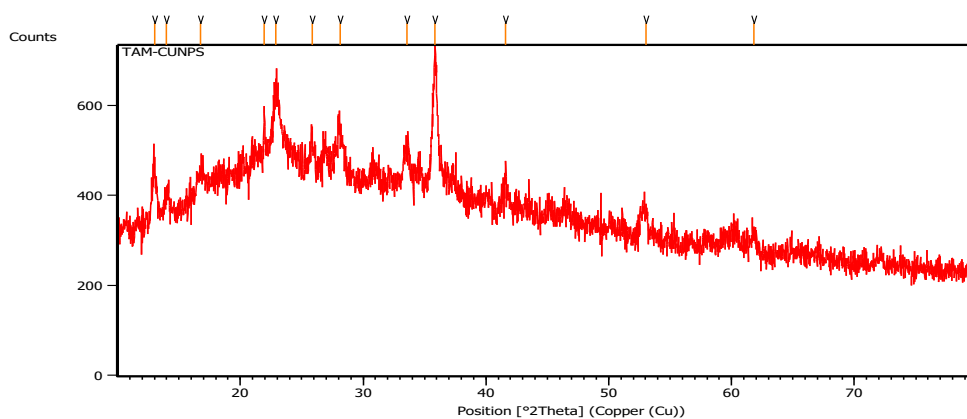
Central Composite Design (CCD), a widely used Response Surface Methodology (RSM) tool, enables efficient process optimization by capturing linear, interaction, and quadratic effects with a minimal number of experimental trials (Jain et al., 2007; Agarwal et al., 2016). In this study, a rotatable CCD was implemented, consisting of 30 experimental runs, integrating factorial, axial (“star”), and center points to ensure uniform prediction accuracy across the design space (Sowjanya et al., 2023). The optimization focused on four independent variables such as initial MG dye concentration (A, mg/L), adsorbent dosage (B, g), solution pH (C), and temperature (D, K) modeled using a second-order quadratic polynomial in Design-Expert v13, with the full CCD matrix presented in Table 1. Adsorption performance was quantified as the percentage removal of MG. ANOVA was used to confirm the model's adequacy; strong predictive performance was indicated by significant model terms and an insignificant lack-of-fit. The response surface model's dependability was supported by diagnostic tests that confirmed normality, constant variance, and the lack of significant outliers. These tests included residual plots and normal probability.

Table 1: Matrix for a 2-factor Central Composite Design (CCD)

Factor	Name	Units	Lower Limit	Upper Limit	Coded Low	Coded High
A	Concentration, C_o	mg/L	10.0	30.0	-1 ↔ 15.0	+1 ↔ 25.0
B	Dosage of adsorbent, w	g/L	0.3	0.7	-1 ↔ 0.4	+1 ↔ 0.6
C	Solution pH		4.0	8.0	-1 ↔ 5.0	+1 ↔ 7.0
D	Temperature, T	K	308.0	328.0	-1 ↔ 313.0	+1 ↔ 323.0

2.5 Characterization of TA-doped Cu nanoparticles

Using XRD, SEM, FTIR, and BET, the structural and surface characteristics of copper nanoparticles doped with TA seed extract were carefully examined. The XRD pattern of TA–CuNPs shown in Fig. 1 exhibits broad, low-intensity features characteristic of nanostructured copper-based materials, with the principal reflections appearing at $2\theta \approx 21.96^\circ$, 22.88° , 28.11° , and 35.86° , the latter showing the highest relative intensity. Although the pattern lacks the sharp, well-defined peaks typical of bulk FCC Cu, the observed maxima near 35.8° and 41.5° may be attributed to mixed copper oxide phases most closely resembling CuO/Cu₂O signatures rather than metallic Cu, given the lack of reflections matching standard Cu (JCPDS 04-0836). The strong background scattering and the broadening of all peaks (FWHM $0.33\text{--}0.60^\circ$) further suggest highly dispersed, well crystalline nanoparticles, which are consistent with synthesis mediated by phytochemicals. SEM images (Fig. 2a, b) depict chiefly spherical, porous particulates with an approximate mean size of 500 nm an architecture conducive to enhanced adsorption. For full analytical transparency, the image should present scale bars alongside the operating conditions such as accelerating voltage of 15.0 kV and working distance of 10.24 mm. Together, these findings show that TA–CuNPs have the high surface area and crystallographic stability needed for effective dye adsorption. The FTIR spectra of TA–CuNPs before and after MG adsorption, presented in Fig. 3a, b exhibit modest but distinct shifts in the O–H/N–H stretching region from 3483 to 3472 cm^{-1} and C–N/C–O region from 1397 to 1388 cm^{-1} regions, indicating the participation of surface hydroxyl and amine groups in dye binding. These trends are consistent with earlier reports on phytochemical-capped metal nanoparticles [Eid et al., 2023; Ejeta et al., 2024]. Spectra were recorded from $4000\text{--}400\text{ cm}^{-1}$ at 4 cm^{-1} resolutions, enabling reliable identification of adsorption-induced vibrational changes. Such findings align with the well-established function of FTIR in clarifying surface alterations and functional group involvement during adsorption in systems of green-synthesized nanoparticles. The pore volume of the adsorbent and surface area TA-CuNPs were analyzed using a surface area analyzer. BET nitrogen adsorption analysis at 77 K confirmed a microporous structure (pore diameter 1.795 nm) with a surface area of $15.259\text{ m}^2/\text{g}$ and pore volume of $0.073\text{ cm}^3/\text{g}$, while Fig. 4a, b presents the corresponding pore-size distribution and N₂ adsorption–desorption isotherms.

**Fig. 1: X-ray diffraction (XRD) pattern of TA-CuNPs.**

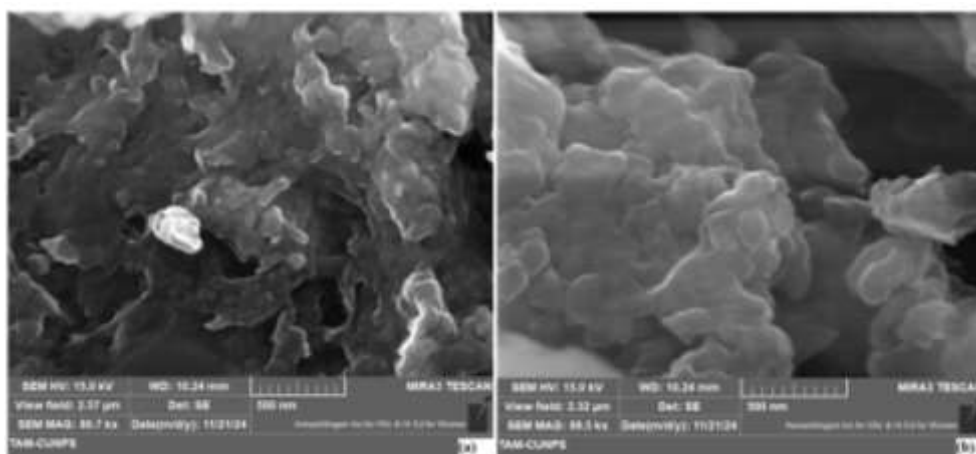


Fig. 2. Scanning Electro Microscope (SEM) image of TA-CuNPs.

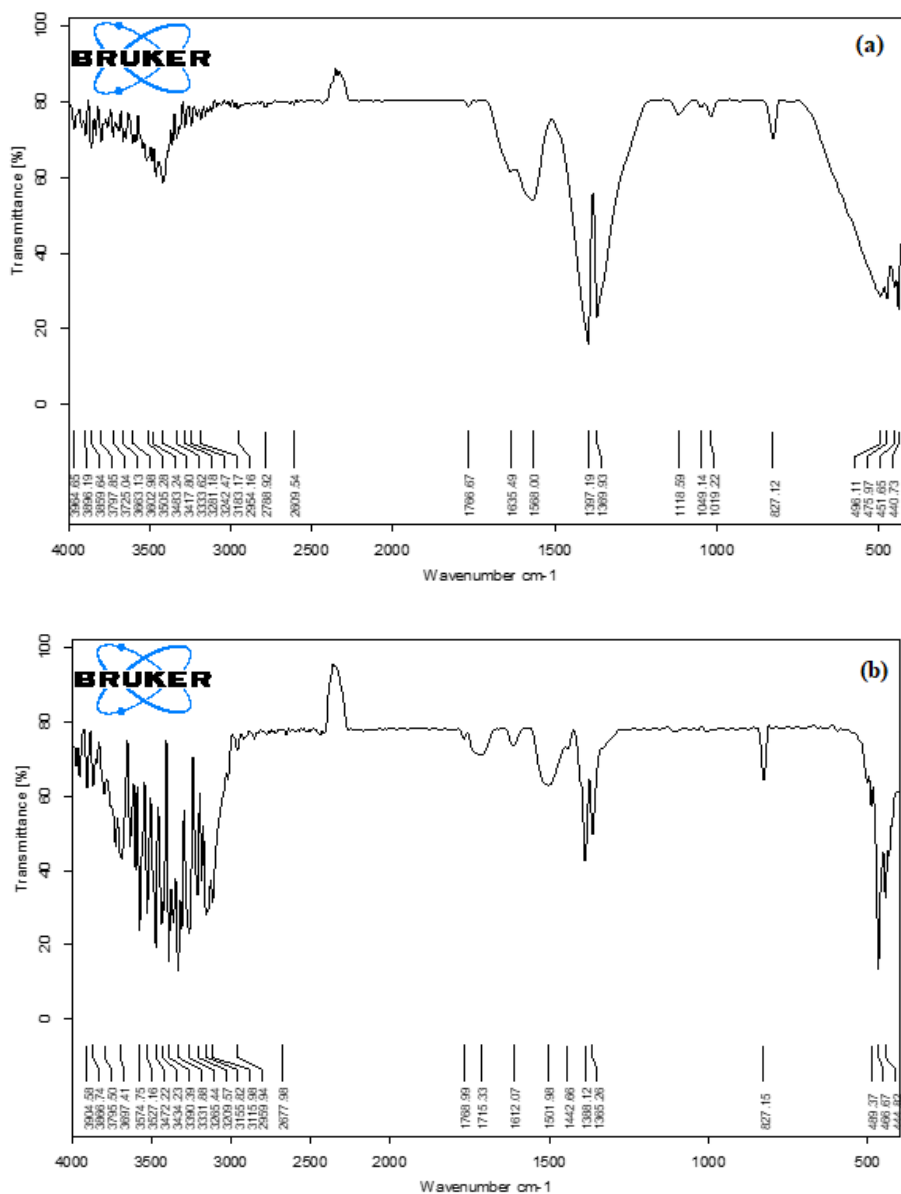


Fig. 3. (a & b). FTIR spectrum of TA-CuNPs adsorbent before & after MG adsorption.

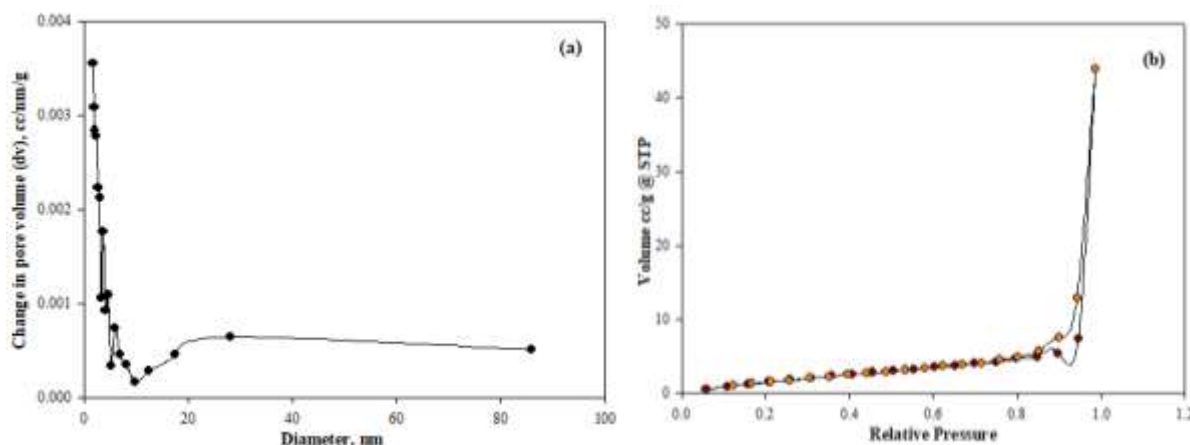


Fig. 4. (a). BET pore size distribution; (b). BET plot of the N₂ adsorption–desorption isotherm.

3. RESULTS AND DISCUSSION

3.1 Contact Time Effect on MG Adsorption

The effects of MG adsorption on TA-CuNPs were investigated for 5–60 minutes at pH 6, 308 K, 100 mg/L, and 0.4 g/L dosage. A sharp initial uptake was observed, with the system reaching equilibrium at approximately 40 minutes shown in Fig. 5a. This rapid early stage results from the abundance of readily accessible active sites and dominant film diffusion, which facilitates fast dye transfer to the nanoparticle surface. The plateau at 40 minutes indicates a shift in the rate-controlling mechanism: as surface sites become progressively occupied, intraparticle (pore) diffusion becomes the limiting step, slowing further adsorption. Thus, the equilibrium time reflects a combined effect of surface site saturation and the transition from rapid film diffusion to slower pore diffusion. This trend demonstrates the strong adsorption capacity and efficient kinetics of TA-CuNPs, comparable to other advanced nanocomposite adsorbents.

3.2 Adsorbent Dosage's Effect on MG Removal

The MG removal efficiency of TA-CuNPs increased from 89.7% to 91.4% as the dosage was raised from 0.1 to 0.8 g/L under fixed conditions (40 min, pH 6.8, 100 mg/L MG, and 308 K). However, the efficiency plateau observed beyond 0.5 g/L Fig. 5b indicates that additional adsorbent no longer enhances performance. At higher concentrations, nanoparticles tend to agglomerate, which leads to overlapping active sites and a reduction in the accessible surface area. Additionally, this aggregation creates a screening effect that decreases the number of effective adsorption sites and restricts dye diffusion toward inner pores. Recent studies on nanocomposite adsorbents, such as copper-ferrite/calcium alginate nanocomposites (Hassan, A.F. et al., 2024) and bio-fabricated CuO nanoparticles (Ejeta, B.A. et al., 2024) used for MG removal, showed such dosage-dependent saturation behavior, where excessive adsorbent mass resulted to diminished surface availability and diffusion limitations.

3.3 Effect of Solution pH on MG Adsorption

pH strongly affects MG adsorption by regulating both dye ionization and the surface charge of TA-CuNPs. Experiments conducted between pH 3–8 (308 K, 100 mg/L MG, 50 min) showed maximum removal at pH 6 as displayed in Fig. 5c. At this pH, the zeta potential of TA-CuNPs becomes sufficiently negative, promoting strong electrostatic attraction with cationic MG. The proton competition for active sites is the cause of reduced adsorption at pH < 6, whereas excess negative charge at higher pH probably causes electrostatic repulsion and restricts uptake. Thus, pH 6 was selected as the optimum for further experiments.

3.4 Effect of Initial Dye Concentration on MG Adsorption

The effects of initial MG concentration (20–100 mg/L) on adsorption by TA-CuNPs was evaluated under experimental conditions (pH 6, 308 K, 40 min). The percentage removal decreased as the dye concentration increased, as seen in Fig. 5d. At low concentrations, the high concentration gradient provides a strong driving force for mass transfer, allowing MG molecules to be efficiently captured by the available active sites. With increasing concentration, however, these sites rapidly become occupied, and the driving force is no longer sufficient to overcome site saturation. This behavior is consistent with Langmuir monolayer adsorption, in which the removal efficiency decreases at high MG levels as the surface gets closer to its maximum loading capacity.

3.5 Kinetic Study of MG Adsorption on TA-CuNPs

The adsorption kinetics of malachite green onto TA-CuNPs were best described by the pseudo-second-order (PSO) model under optimal conditions (pH 6, 318 K, 0.5 g/L adsorbent, 100 mg/L MG). The PSO model showed an excellent fit, with $R^2 = 0.999$ and close agreement between calculated and experimental q_e values. Furthermore, a removal efficiency of 92.09% was achieved at an equilibrium time of 40 minutes, confirming the high adsorption performance of the system. In contrast, the pseudo-first-order model produced higher χ^2 and RMSE values, confirming its poorer suitability. The superior performance of the PSO model indicates chemisorption as the dominant rate-controlling step, driven by electron sharing or exchange between MG molecules and surface sites on the nanoparticles. This mechanism aligns with potential coordination interactions between Cu and *Tamarindus indica*-derived functional groups (–OH, –COOH, phenolic groups). The kinetic parameters are summarized in Table 2, and the kinetic fits are displayed in Fig. 6a, b.

3.6. Analysis of Adsorption Isotherms

The adsorption equilibrium of MG on TA-CuNPs was modelled using the Langmuir and Freundlich isotherms are presented Fig. 7a, b. The Langmuir model showed the strongest agreement with the data ($R^2 = 0.999$), confirming that MG interacts with a uniform surface through monolayer chemisorption. This finding is reinforced by the Langmuir separation factor ($R_L = 0.336$), which remained between 0 and 1, indicating favorable adsorption. The predicted q_{max} (243.902 mg/g) also aligned closely with the experimental q_e (208.333 mg/g). Although the Freundlich model ($R^2 = 0.979$) suggests mild surface heterogeneity at higher concentrations, the Langmuir isotherm clearly dominates. The isotherm constants are summarized in Table 3, and Table 4 compares the adsorption performance of TA-CuNPs with other reported adsorbents.

3.7 Analysis of Thermodynamics

Using an initial MG concentration of 20 mg/L, the thermodynamic behavior of adsorption onto TA-CuNPs was examined at 303–318 K. The Van't Hoff plot ($\ln K_c$ vs. $1/T$) in Fig. 8 showed strong linearity ($R^2 = 0.9903$), allowing ΔH° and ΔS° to be calculated from its slope and intercept; the resulting values are listed in Table 5. MG uptake occurs spontaneously at all temperatures under investigation, as confirmed by the consistently negative ΔG° values. The positive ΔH° indicates an endothermic process, which reflects the energy required for MG molecules to overcome hydration forces, reorganize interfacial species, and penetrate the nanoparticle pores; this process that may involve minor changes in surface functionalities during binding. Due in large part to the displacement of structured water molecules and the increased configurational freedom gained as MG occupies adsorption sites on the TA-CuNPs surface, the significantly high ΔS° indicates a marked increase in interfacial disorder. This combined enthalpy–entropy profile explains why adsorption becomes stronger at higher temperatures: thermal input increases molecular mobility, facilitates removal, and allows for more efficient dye–surface interactions, all of which improve overall adsorption efficiency.

Table 2: MG's adsorption kinetics onto TA-CuNPs were determined.

Kinetic model	k_1 (1/min)	k_2 , (g/mg. min)	q_e (mg/g)	R^2
Pseudo-first-order	0.0956	--	151.836	0.9372
Pseudo-second-order	--	0.00082	208.333	0.9990

Table 3: Adsorption isotherm parameters for MG uptake on TA-CuNPs derived from the model.

Langmuir Isotherm modeling		Freundlich Isotherm modeling	
b (L/mg)	0.1017	K_f ($\text{mg}^{1-1/n}\text{L}^{1/n}\text{g}^{-1}$)	27.5913
q_{max} (mg/g)	243.902	n	1.5745
R^2	0.999	R^2	0.979

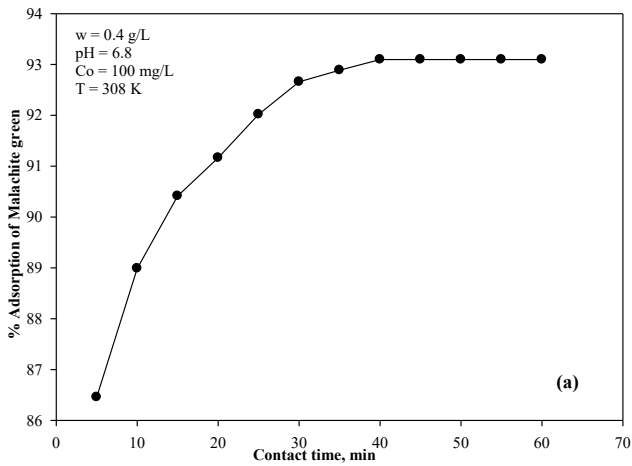


Fig. 5a. Effect of contact time on MG adsorption

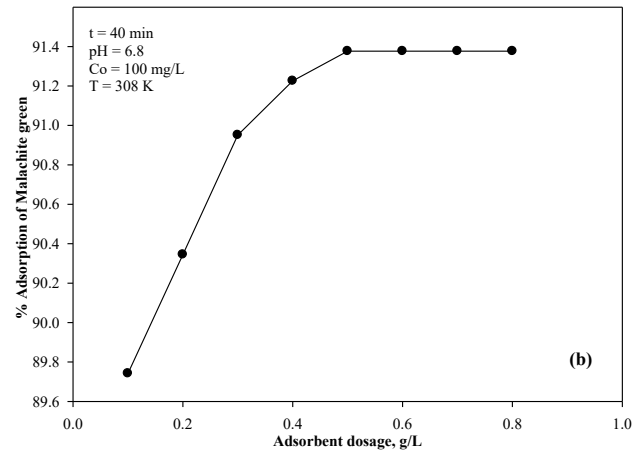


Fig. 5b. Effect of adsorbent dosage on MG adsorption

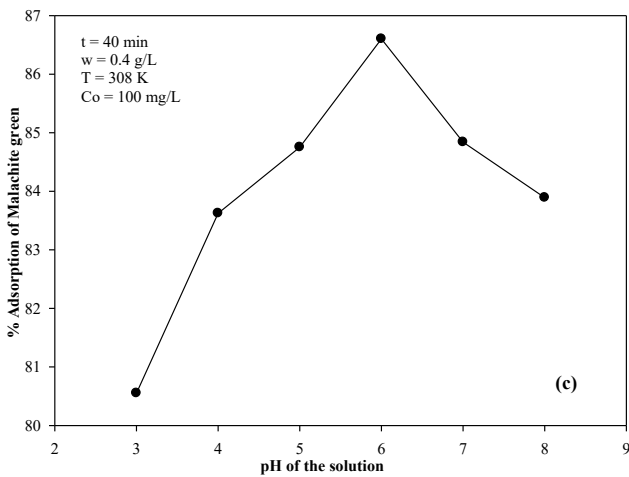


Fig. 5c. Effect of pH on MG adsorption

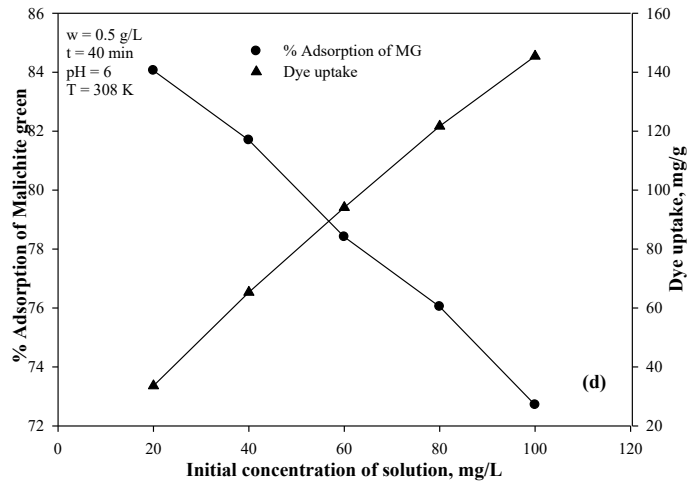


Fig. 5d. Effect of initial dye concentration on MG adsorption

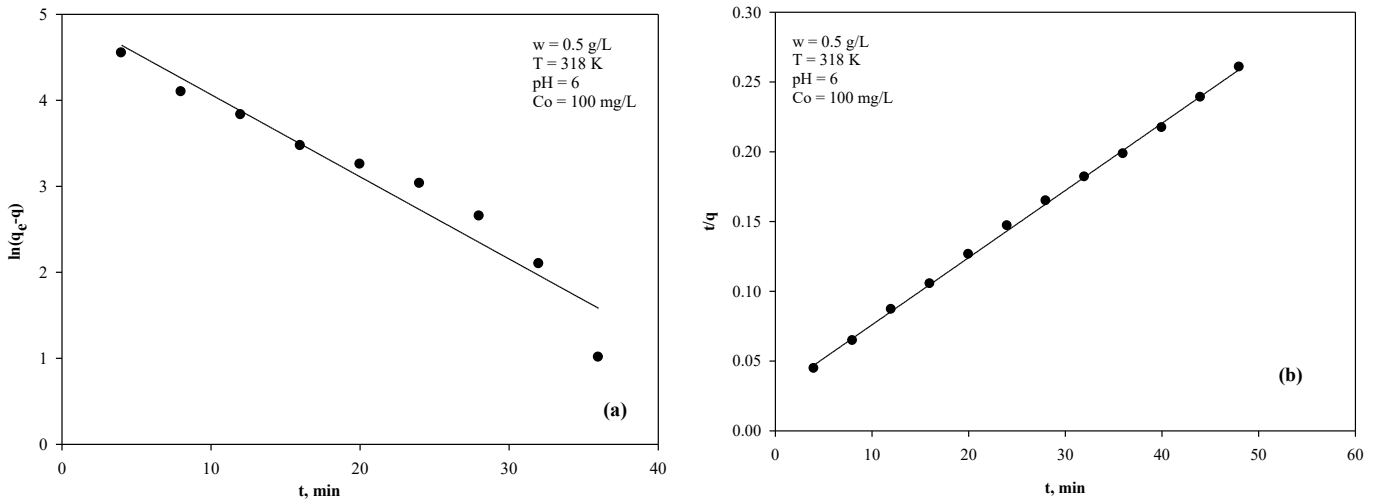


Fig. 6. Kinetic study models for MG adsorption: (a). Pseudo-First-order; (b). Pseudo-Second-order.

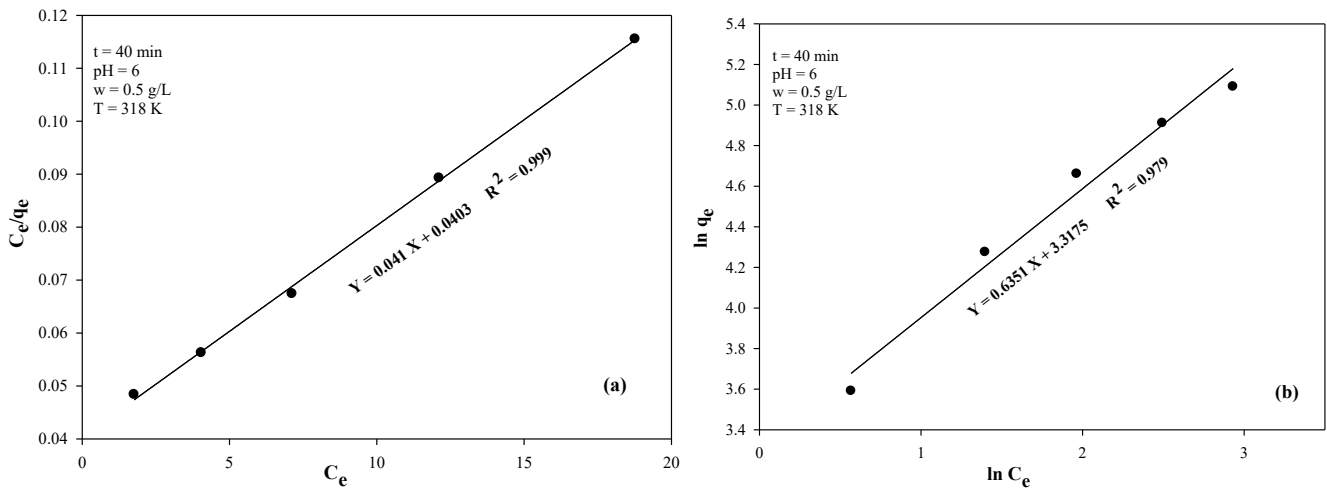


Fig. 7. Adsorption isotherm models for MG adsorption: (a). Langmuir isotherm; (b). Freundlich isotherm.

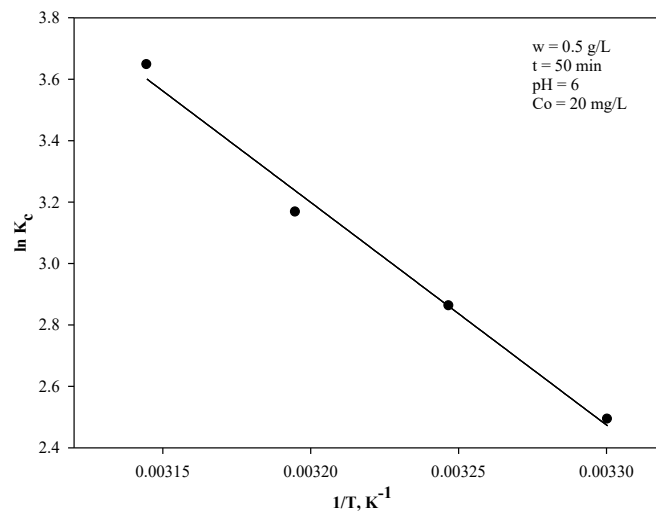


Fig. 8. The thermodynamic evaluation for adsorption of Malachite green.

Table 4: MG removal from aqueous solution using the relative adsorption capacities of different adsorbents.

S.No.	Type of Adsorbent/Bio-sorbent	Max Dye uptake, mg/g	Reference
1	Spent tea leaves-Activated carbon (STAC)	256.40	Emine Akar et al., 2013
2	Leaves of solanum tuberosum potato plant waste	33.33	Gupta N et al., 2011
3	Pine apple stem	119.05	Hamed B. H. et al., 2009
4	Dead leaves of platanus vulgaris	85.47	Hamdaouia. O et al., 2008
5	Activated Carbon Supported Zinc Sulfide–Copper Nanocomposite (ZnS–Cu–NP/AC)	168.10	Mehdi D et al., 2015
6	Activated Carbon Supported Silver Nanoparticles (Ag–NP/AC)	95.20	Mortazavi K. et al., 2016
7	Halloysite nanotubes (HNT)	74.95	Turkan A & Huseyin E, 2022
8	Cellulose nanofibers and silver nanoparticles	142.00	Nagalakshmi Ch et al., 2021
9	TA-doped Cu nanoparticles (TA-CuNPs)	243.90	Present study

Table 5: Thermodynamic variables (ΔG° , ΔH° , and ΔS°) for adsorption of MG onto TA-CuNPs.

Temperature, (K)	Change in Gibbs-Free Energy, ΔG° (kJ/mol)	Change in Enthalpy, ΔH° (kJ/mol)	Change in Entropy, ΔS° (J/mol.K)
308	-6.281		
313	-7.328		
318	-8.243	60.295	219.534
323	-9.628		

3.8. Process Optimization Using Response Surface Methodology (RSM)

The “Central Composite Design” consisting of 30 experimental runs were implemented to optimize the % removal of MG using TA-doped copper nanoparticles (TA-CuNPs). The experimental framework incorporated four independent factors—initial MG dye concentration (A), dosage of adsorbent (B), solution pH (C), and temperature (D)—were systematically varied to investigate both their main effects and interaction influences on the adsorption efficiency. The coded and actual levels of these factors, along with the corresponding experimental responses, are summarized in Table 6. A quadratic (2nd) polynomial regression model was constructed to correlate the % removal of MG with the coded process variables, offering an in-depth depiction of the adsorption behavior under the investigated operational condition.

$$\begin{aligned} \% \text{Adsorption of MG} = & 91.35 - 0.1688 \times A - 0.3304 \times B + 0.6937 \times C + 0.1729 \times D + 0.1856 \times AB + \\ & 0.0019 \times AC + 0.4419 \times AC + 0.0806 \times BC + 0.3256 \times BD + 0.2669 \times CD + \\ & 3.28 \times A^2 - 3.42 \times B^2 - 3.52 \times C^2 - 2.08 \times D^2 \end{aligned} \quad (9)$$

In the regression analysis, factors were coded to -1 and +1 to enable direct comparison of their relative effects through standardized regression coefficients. With a significant Model F-value of 1755.38 and $p < 0.0001$, the robustness of the quadratic CCD model was confirmed by ANOVA in Table 7. This indicates that all linear, interaction (AB, AD, BD, and CD), and quadratic terms were statistically significant, and that such a large F-value is highly unlikely to arise from noise.

Additionally, The model has sufficient predictive power to reliably navigate the experimental design space, as evidenced by the high Adequate Precision of 121.889 and the close alignment of adjusted (0.9988) and predicted (0.9965) R^2 values, which show an excellent signal-to-noise ratio well above the threshold of 4. 19.85 mg/L MG concentration, 0.498 g/L adsorbent dosage, pH 6.18, and 318.24 K were found to be the optimal conditions through optimization using the desirability function depicted in Fig. 9a and the close match between experimental and predicted values are shown in Fig. 9b further support the dominance of these interactions and validate the model for reliable process optimization. This resulted in a predicted removal efficiency of 91.37% (desirability = 1.0), a value that is practically relevant for real-world wastewater treatment applications. Under experimental conditions, an actual removal efficiency of 92.09% was achieved, further validating the model's reliability and practical applicability. Due to their control over surface charge and active-site availability, the 3D response surfaces and contour plots are revealed that pH and adsorbent dosage had the strongest effects. Conversely, interactions involving dosage–pH and dosage–temperature were the most prominent, indicating a synergistic enhancement of adsorption capacity under conditions favouring electrostatic attraction and endothermic uptake. The strong curvature in surface and Contour plots are presented in Fig. 10a-f and Fig.11a-f.

Table 6: Central Composite Design (CCD) matrix showing the experimental factors and corresponding responses for MG adsorption.

Run	Initial MG Dye Concentration (A) : mg/L	Adsorbent dosage (B): g/L	Solution pH (C):	Temperature (D): K	Experimental value	Predicted value
1	15	0.4	5	313	79.86	79.88
2	25	0.4	5	313	78.54	78.38
3	15	0.6	5	313	78.22	78.13
4	25	0.6	5	313	77.43	77.28
5	15	0.4	7	313	80.63	80.67
6	25	0.4	7	313	78.95	79.08
7	15	0.6	7	313	79.35	79.15
8	25	0.6	7	313	78.15	78.30
9	15	0.4	5	323	78.42	78.26
10	25	0.4	5	323	78.21	78.43
11	15	0.6	5	323	77.83	77.71
12	25	0.6	5	323	78.68	78.63
13	15	0.4	7	323	79.85	80.01
14	25	0.4	7	323	80.12	80.19
15	15	0.6	7	323	79.65	79.79
16	25	0.6	7	323	80.82	80.71
17	10	0.5	6	318	78.52	78.31

18	30	0.5	6	318	77.95	77.90
19	20	0.3	6	318	78.52	78.57
20	20	0.7	6	318	76.78	76.99
21	20	0.5	4	318	75.68	75.87
22	20	0.5	8	318	78.84	78.65
23	20	0.5	6	308	82.60	82.68
24	20	0.5	6	328	83.45	83.37
25	20	0.5	6	318	91.35	91.35
26	20	0.5	6	318	91.35	91.35
27	20	0.5	6	318	91.35	91.35
28	20	0.5	6	318	91.35	91.35
29	20	0.5	6	318	91.35	91.35
30	20	0.5	6	318	91.35	91.35

Table 7: ANOVA for the quadratic model to describing MG adsorption onto TA-CuNPs.

Source of Variation	Sum of the Squares (SS)	The Degrees of freedom (df)	The Mean Square (MS)	F-value	p-value	
Model	792.38	14	56.60	1755.38	< 0.0001	significant
A:Initial concentration of the MG dye	0.6834	1	0.6834	21.20	0.0003	
B: Adsorbent dosage	2.62	1	2.62	81.26	< 0.0001	
C: Solution pH	11.55	1	11.55	358.25	< 0.0001	
D:Temperature	0.7176	1	0.7176	22.26	0.0003	
AB	0.5513	1	0.5513	17.10	0.0009	
AC	0.0001	1	0.0001	0.0017	0.9672	
AD	3.12	1	3.12	96.89	< 0.0001	
BC	0.1040	1	0.1040	3.23	0.0927	
BD	1.70	1	1.70	52.62	< 0.0001	
CD	1.14	1	1.14	35.34	< 0.0001	
A ²	294.81	1	294.81	9143.33	< 0.0001	
B ²	321.70	1	321.70	9977.29	< 0.0001	
C ²	340.27	1	340.27	10553.48	< 0.0001	
D ²	118.77	1	118.77	3683.74	< 0.0001	
Residual Error	0.4836	15	0.0322			
Lack of Fit	0.4836	10	0.0484			
Pure Error	0.0000	5	0.0000			
Corrected Total	792.86	29				

Adjusted R² 0.9988
 Predicted R² 0.9965
 Adeq Precision 121.8890

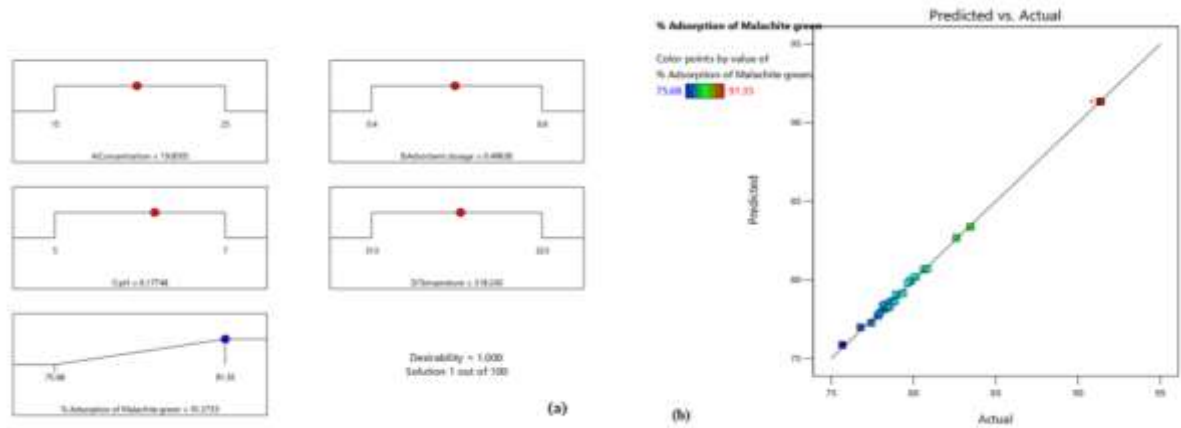


Fig. 9 (a). Ramp plot illustrating the optimized conditions for MG adsorption onto TA-CuNPs; (b). Comparison of the CCD Model's predicted and experimental values.

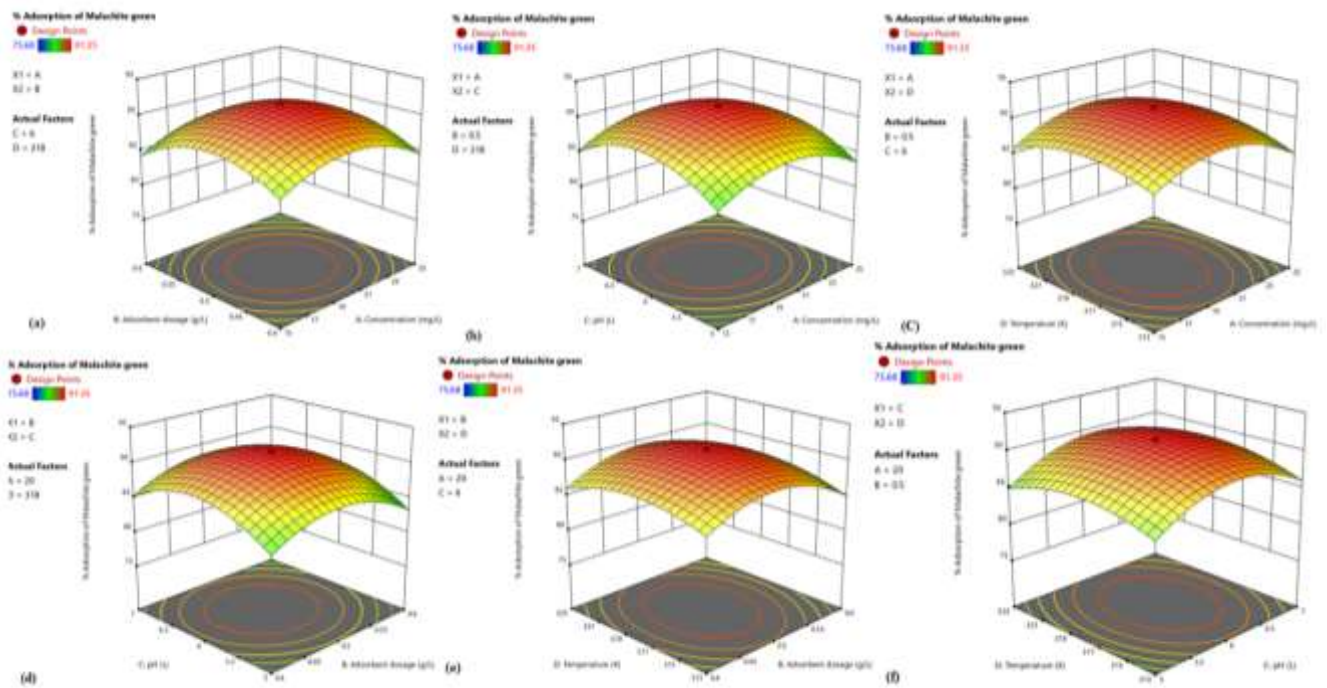


Fig. 10. 3D response-surface plots illustrating the interactive effects of (a) concentration and adsorbent dosage; (b) concentration and pH; (c) concentration and temperature; (d) adsorbent dosage and pH; (e) adsorbent dosage and temperature; (f) pH and temperature on the percentage removal of malachite green by TA-CuNPs.

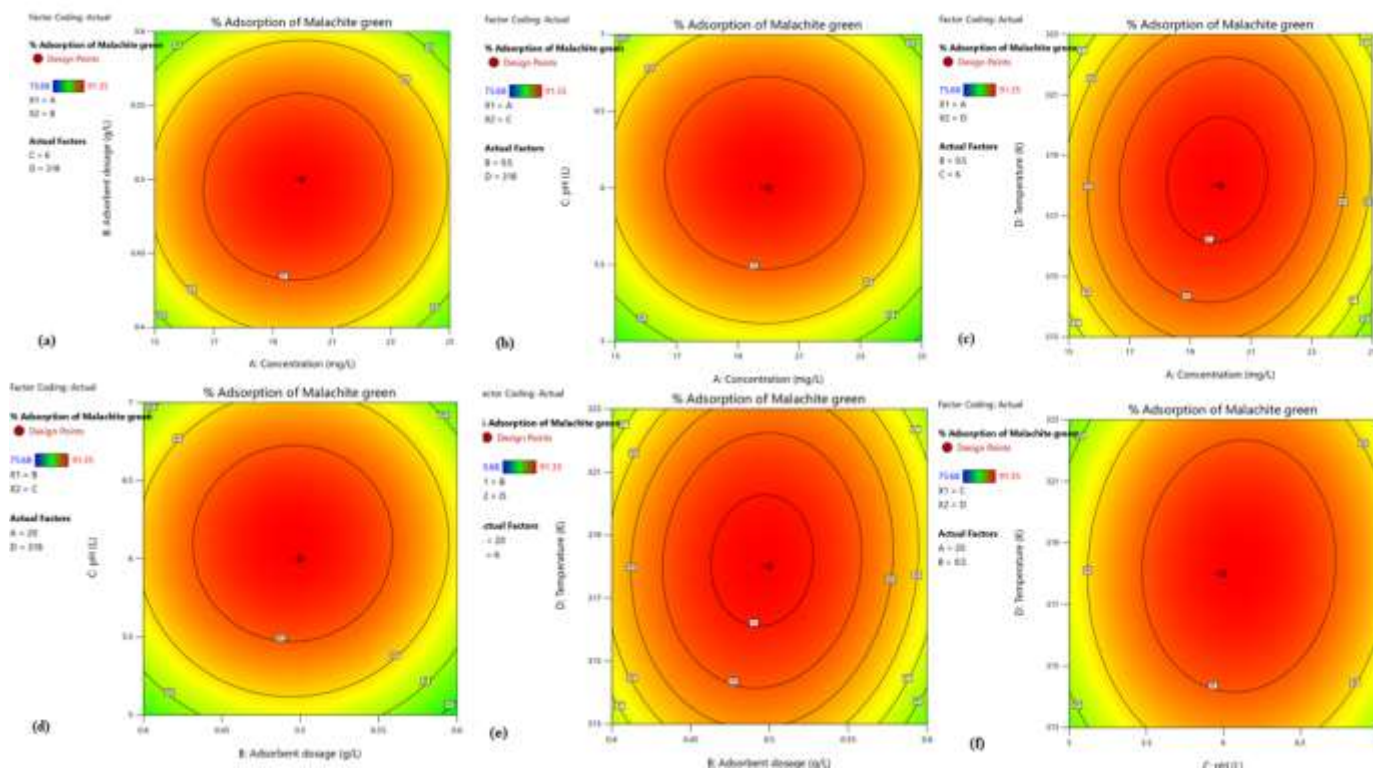


Fig. 11. 3D contour plots illustrating the interactive effects of (a) concentration and adsorbent dosage; (b) concentration and pH; (c) concentration and temperature; (d) adsorbent dosage and pH; (e) adsorbent dosage and temperature; (f) pH and temperature on the percentage removal of malachite green by TA-CuNPs.

4. CONCLUSION

Synthesized by co-precipitation, TA-doped copper nanoparticles (TA-CuNPs) were extensively characterized (SEM, XRD, FTIR, and BET), confirming their functional surface groups and porous morphology. In this study, TA-CuNPs exhibited efficient removal of malachite green, with adsorption strongly governed by pH, concentration, dosage, and contact time, yielding a Langmuir monolayer capacity of 243.90 mg/g. The process followed pseudo-second-order kinetics and showed spontaneous, endothermic behavior, with optimum batch conditions identified at pH 6 and 0.5 g/L. RSM-based CCD optimization further defined the ideal operating parameters as 19.85 mg/L MG, 0.498 g/L adsorbent, pH 6.18, and 318 K, achieving the maximum removal efficiency, while the quadratic model demonstrated strong statistical validity through high R^2 and low error values. Comparative assessment with reported adsorbents confirmed the competitive performance of TA-CuNPs. To facilitate practical scale-up, further studies should thoroughly investigate multi-cycle regeneration, the impact of co-existing ions, breakthrough behavior under continuous-flow or fixed-bed operation, and cost-benefit viability in comparison to commercial adsorbents.

Author Contributions: P. Anil Kumar handled data curation, formal analysis, and experimental investigations. Pulipati King guided the work through conceptualization, methodology, and supervision; D. Appala Naidu guided the work through conceptualization, methodology, and supervision; Meena Vangalapati provided critical input in conceptualization, methodology, and overall supervision; Alpitha Suhasini J and Sarva Rao B oversaw the visualization, wrote the manuscript, and edited and reviewed it to make it better.

Funding: No funding from outside was obtained.

Data Availability: This manuscript includes all of the data and materials.

Conflict of Interest: No conflicts of interest are disclosed by the authors.

Ethical Approval: Not applicable, considering that neither human nor animal subjects were used in this investigation.

REFERENCES

1. Bandela Sowjanya, Pulipati King, Meena Vangalapati, Venkata Ratnam Myneni, (2023), Copper-doped zinc oxide nanoparticles: synthesis, characterization, and application for adsorptive removal of toxic azo dye, *Hindawi, International Journal of Chemical Engineering*, Volume 2023, Article ID 8640288. <https://doi.org/10.1155/2023/8640288>
2. Bashanaini SM, (2019), Removal of malachite green dye from aqueous solution by adsorption using modified and unmodified local agriculture waste, *Sci J Anal Chem*, 7(2):42-56. DOI: [10.11648/j.sjac.20190702.12](https://doi.org/10.11648/j.sjac.20190702.12)
3. Chi-Hui Tsou, Zheng-Lu Ma, Manuel Reyes De Guzman, Lei Zhao, Juan Du, Wilfred Emori, Chen Gao, Yanchun Zhao, Tao Yang, Jintian Wu, (2022), High-performance antibacterial nanocomposite films with a 3D network structure prepared from carboxylated graphene and modified polyvinyl alcohol, *Progress in Organic Coatings*, Volume 166, 106805, ISSN 0300-9440. (<https://doi.org/10.1016/j.porgcoat.2022.106805>)
4. Eid, A. M., Fouda, A., Hassan, S. E.-D., Hamza, M. F., Alharbi, N. K., Elkelish, A., Alharthi, A., & Salem, W. M., (2023), Plant-Based Copper Oxide Nanoparticles: Biosynthesis, Characterization, Antibacterial Activity, Tanning Wastewater Treatment, and Heavy Metals Sorption, *Catalysts*, 13(2), 348. (<https://doi.org/10.3390/catal13020348>)
5. Ejeta, B.A., Aaga, G.F., Fereja, W.M. *et al.*, (2024), Biofabrication of highly effective and easily regenerated CuO nanoparticles as adsorbents for Congo red and malachite green removal, *Sci Rep* 14, 24116. (<https://doi.org/10.1038/s41598-024-74974-5>)
6. Emine Akar, Aylin Altinişik, Yoldaş Seki, (2013), Using of activated carbon produced from spent tea leaves for the removal of malachite green from aqueous solution, *Ecological Engineering*, Vol 52, PP 19-27. (<https://doi.org/10.1016/j.ecoleng.2012.12.032>)
7. Figen Gündüz, Bahar Bayrak, (2018), Synthesis and performance of pomegranate peel-supported zero-valent iron nanoparticles for adsorption of malachite green, *Desalination and Water Treatment*, Volume 110, Pages 180-192, ISSN 1944-3986. (<https://doi.org/10.5004/dwt.2018.22185>)
8. Gupta, N., Atul, K. Kushwah. Chattopadhyaya. M. C., (2011), Application of potato plant wastes for the removal of methylene blue and malachite green dye from aqueous solution, *Arabian Journal of Chemistry*, 1878-5352. (DOI: [10.1016/j.arabjc.2011.07.0210](https://doi.org/10.1016/j.arabjc.2011.07.0210))

9. Hamdaouia. O., Saoudi. F., China. M., Naffrechoux. E., (2008), Sorption of Malachite green by a novel sorbent Dead leaves of plane tree; equilibrium and kinetic modeling, *Chem. Engg*, 143, 73-84. (<http://dx.doi.org/10.1016/j.cej.2007.12.018>)
10. Hamed B. H. Hamoed. Krishni. R. R., Sata, S. A., (2009), A novel agricultural waste adsorbent for the removal of cationic dye from aqueous solutions, *Journal of Hazard Materials*, 162, 305-311. (DOI: [10.1016/j.jhazmat.2008.05.036](https://doi.org/10.1016/j.jhazmat.2008.05.036))
11. Hassan, A.F., El-Naggar, G.A., Braish, A.G. et al., (2024), Utilization of Synthesized Copper Ferrite/Calcium Alginate Nanocomposite for Adsorption and Photocatalytic Degradation of Malachite Green. *J Inorg Organomet Polym* 34, 190–206. <https://doi.org/10.1007/s10904-023-02806-6>
12. Hussien Hamad, M.T.M., (2023), Optimization study of the adsorption of malachite green removal by MgO nano-composite, nano-bentonite and fungal immobilization on active carbon using response surface methodology and kinetic study. *Environ Sci Eur* 35, 26. <https://doi.org/10.1186/s12302-023-00728-1>
13. Jain, R., Mathur, M., Sikarwar, S., Mittal, A., (2007), Removal of the hazardous dye rhodamine B through photocatalytic and adsorption treatments. *J. Environ. Manag.* 85, 956–964. <https://doi.org/10.1016/j.jenvman.2006.11.002>
14. Kumar, K.M., Mandal, B.K., Kumar, K.S., Reddy, P.S., Sreedhar, B., (2013), Bio-based green method to synthesise palladium and iron nanoparticles using terminalia chebula aqueous extract, *Spectrochim. Acta A* 102,128–133. (<https://doi.org/10.1016/j.saa.2012.10.015>)
15. Mehdi Dastkhon, Mehrorang Ghaedi, Arash Asfaram, Alireza Goudarzi, Sanaz Mehdizadeh Langroodi, Inderjeet Tyagi, Shilpi Agarwal, Vinod Kumar Gupta, (2015), Ultrasound assisted adsorption of malachite green dye onto ZnS-Cu-NP-AC: Equilibrium isotherms and kinetic Studies-Response surface optimization, *Separation and Purification Technology*, Vol 156, Part 2, PP 780-788. (<https://doi.org/10.1016/j.seppur.2015.11.001>)
16. Mortazavi, K., Rajabi, H., Ansari, A., Ghaedi, M., & Dashtian, K., (2016), Preparation of silver nanoparticle loaded on activated carbon and its application for removal of malachite green from aqueous solution, *Synthesis and Reactivity in Inorganic, Metal-Organic, and Nano-Metal Chemistry*. (DOI: [10.1080/15533174.2016.12286700](https://doi.org/10.1080/15533174.2016.12286700))
17. Muinde, V., Onyari, J. , Wamalwa, B. , Wabomba, J. and Nthumbi, R., (2017), Adsorption of Malachite Green from Aqueous Solutions onto Rice Husks: Kinetic and Equilibrium Studies, *Journal of Environmental Protection*, 8, 215-230. (DOI: [10.4236/jep.2017.83017](https://doi.org/10.4236/jep.2017.83017))

18. Nadagouda, M.N., Castle, A.B., Murdock, R.C., Hussain, S.M., Varma, R.S., (2010), Invitrobiocompatibility of nanoscale zero valent iron particles (NZVI) synthesized using tea polyphenols, *Green Chem.* 12, 114–122. <https://doi.org/10.1039/B921203P>
19. Nagalakshmi Chinthalapudi, Vindhya Vasini Devi Kommaraju, Mukesh Kumar Kannan, Chitti Babu Nalluri, Swambabu Varanasi, (2021), Composites of cellulose nanofibers and silver nanoparticles for malachite green dye removal from water, *Carbohydrate Polymer Technologies and Applications*, Volume 2, 100098, ISSN 2666-8939. <https://doi.org/10.1016/j.carpta.2021.10009810.1021/la103190n>
20. Njagi, E.C., Huang, H., Stafford, L., Genuino, H., Galindo, H.M., Collins, J.B., Hoag, G.E.Suib, S.L., (2011), Biosynthesis of iron and silver nanoparticles at room temperature using aqueous sorghum bran extract. *Langmuir* 27, 264–271. (DOI: [10.1021/la103190n](https://doi.org/10.1021/la103190n))
21. Philip, D., (2010), Green synthesis of gold and silver nanoparticles using Hibiscus rosasinensis, *Physica E* 42, 1417–1424. <https://doi.org/10.1016/j.physe.2009.11.081>
22. Poiba, V. R., Sowjanya, B., King, P., & Vangalapati, M. (2023), Removal of methylene blue dye by using synthesised *Grevillea robusta* silver nanoparticles and optimisation of experimental parameters by response surface methodology (central composite design), *Advances in Materials and Processing Technologies*, 10(4), 3013–3027. <https://doi.org/10.1080/2374068X.2023.2192393>
23. Raton Kumar Bishwas, Sabrina Mostofa, Md. Ashraful Alam, Shirin Akter Jahan, (2023), Removal of malachite green dye by sodium dodecyl sulfate modified bentonite clay: Kinetics, thermodynamics and isotherm modeling, *Next Nanotechnology*, Volumes 3-4, 100021, ISSN 2949-8295. <https://doi.org/10.1016/j.nxnano.2023.100021>
24. Shilpi Agarwal, Inderjeet Tyagi, Vinod Kumar Gupta, Somaye Mashhadi, Maryam Ghasemi, (2016), Kinetics and thermodynamics of malachite green dye removal from aqueous phase using iron nanoparticles loaded on ash, *Journal of Molecular Liquids*, Volume 223, Pages 1340-134. <https://doi.org/10.1016/j.molliq.2016.04.039>
25. T. Shahwan, S. Abu Sirriah, M. Nairat, E. Boyacı, A.E. Eroğlu, T.B. Scott, K.R. Hallam, (2011), Green synthesis of iron nanoparticles and their application as a Fenton-like catalyst for the degradation of aqueous cationic and anionic dyes, *Chemical Engineering Journal*, Volume 172, Issue 1, Pages 258-266, ISSN 1385-8947. <https://doi.org/10.1016/j.ccej.2011.05.103>

26. Turkan Altun, Huseyin Ecevit, (2022), Adsorption of malachite green and methyl violet 2B by Halloysite nanotube: Batch adsorption experiments and Box-Behnken experimental design, *Materials Chemistry and Physics*, Vol 291, 126612. (<https://doi.org/10.1016/j.matchemphys.2022.126612>)